

MODELING AND SIMULATION OF ROCK MASS STRESSES FOLLOWING TUNNEL EXCAVATION

**MARIAN-GABRIEL BORDEIANU¹, ZHAO QI²,
LAURA COJANU³, FLORIN DUMITRU POPESCU⁴,**

Abstract: Numerical methods for modeling and simulation are increasingly used in engineering design and verification activities. This trend has led to the development of new calculation methods as well as the emergence of applications aimed at solving problems using the finite element method or discrete finite element method.

The inevitable trend of modernizing calculation methods has also affected the mining industry, particularly in the field of geomechanics. The paper presents a calculation method for determining the stresses that occur in a rock mass after tunnel excavation. In this regard, the Comsol Multiphysics application was used to create a virtual model of a rock mass where a tunnel will be excavated.

The simulation was carried out in two stages: the first stage, where the in-situ stresses due to gravity were determined without considering the plastic characteristics of the material constituting the rock mass, and the second stage, where von Mises stresses and deformations of the model subjected to simulation were determined after the tunnel excavation.

Keywords: underground constructions, Tunnel Boring Machine, stress state, boundary conditions.

1. GENERAL NOTIONS REGARDING UNDERGROUND CONSTRUCTION WORKS

Underground constructions form a distinct category within the field of construction in general. They can be considered the opposite of surface constructions.

The 20th century is marked by the overcrowding of cities. This issue necessitated solving traffic and urban infrastructure challenges through underground constructions, such as underground passages, subways, various underground road

¹ Ph.D. student Eng., University of Petroșani, gabriel.bordeianu@gmail.com

² Ph.D. student Eng., University of Petroșani, zhaoqi0715@hotmail.com

³ Ph.D. student Eng., University of Petroșani, cojanulaura@gmail.com

⁴ Prof. Ph.D. Eng., University of Petroșani, fpopescu@gmail.com

networks, and parking facilities. These requirements have driven the development and refinement of machinery designed for underground construction works.

Figure 1 illustrates such a piece of equipment, which will be used in our country for the modernization of the Apața–Cața railway section in Brașov County (part of the Rhine-Danube European corridor). Figure 2 shows the working method of the TBM (Tunnel Boring Machine).



Fig. 1. TBM used for the modernization of the Apața – Cața railway section, Brașov county



Fig. 2. Excavation mode using the TBM

The underground space can be considered to have the following fundamental characteristics:

- the underground environment provides a location for activities or infrastructure that are difficult, impossible, unprofitable, or undesirable to place above ground from an environmental perspective;
- the underground space offers natural protection for anything placed below the surface;

- the structures created underground shield the external environment from risks or disruptions inherent to certain types of activities;
- the underground space is opaque, with its structures visible only at points of contact with the surface.

Figures 3 and 4 show a formwork for casting the arch of a tunnel in both two-dimensional and three-dimensional views.



Fig. 3. Formwork for casting the arch of a tunnel – 2D view

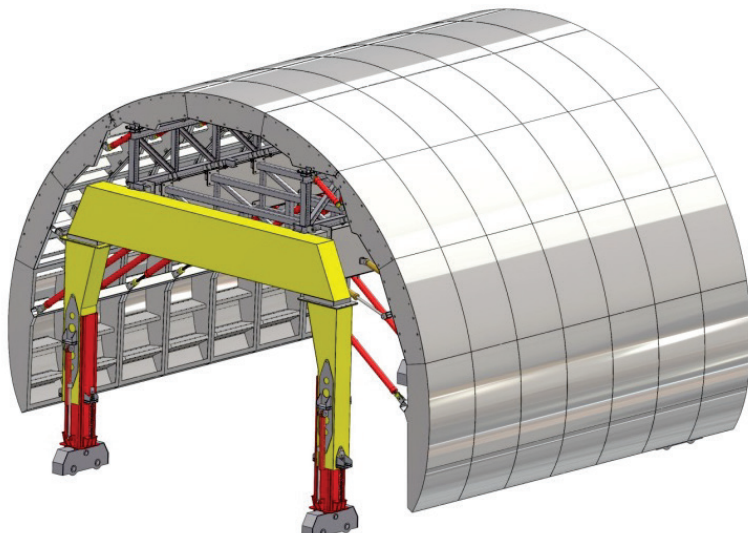


Fig. 4. Formwork for casting the arch of a tunnel – 3D view

2. MODELING AND SIMULATION OF SOIL BEHAVIOR DURING TUNNEL EXCAVATION

The surface, settlement, and width of the plastic region around the tunnel are important parameters required for determining the characteristics of the reinforcements used during excavation. In situ stresses are calculated in two stages. In the first study, the stress state of the soil before excavation is evaluated. In the second study, the elastoplastic behavior after soil removal is assessed, using the stress response calculated in the first study. Soil removal is simulated using the Activation feature of the linear elastic material model. To accelerate the computation, the soil is considered elastic in the first stage, and only in the second stage is the Drucker-Prager soil plasticity model applied. The simulation was performed for a 2D geometry under plane strain conditions.

2.1. Model definition

2.1.1. Definition of the geometric model

The geometry consists of a layer of soil that is 45 m deep and 90 m wide as can be seen in figure 5. A tunnel with a diameter of 10 m is placed here, the center of which is located on the axis of symmetry 20 m below the surface. The 45 m wide base rock is fixed and constrains the movement in the vertical direction. In order to model the infinite extension of the soil in the lateral direction, a roller-type constraint was imposed on the right end of the model.

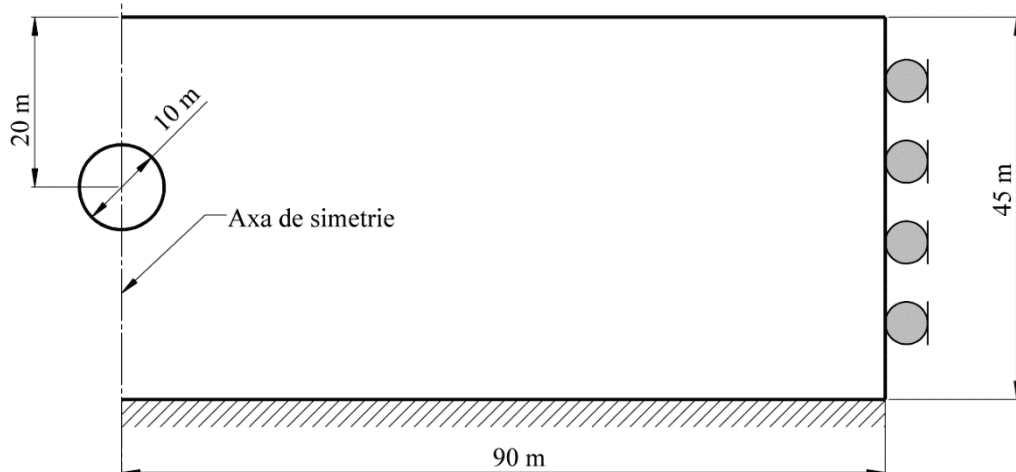


Fig. 5. Dimensions and boundary conditions for the excavated tunnel model

2.1.2. Material properties

The material properties corresponding to the soil are as follows:

- Young's modulus: $E = 12 \text{ MPa}$;
- Poisson's ratio $\nu = 0,495$;

- Cohesion $c = 130 \text{ kPa}$;
- Internal friction angle $\Phi = 30^\circ$.

In the simulation, the Drucker-Prager criterion was used, and the material parameters were harmonized with the Mohr-Coulomb criterion.

2.1.3. Constraints and loads

As mentioned earlier, the lower limit of the analyzed domain has a fixed constraint that prevents vertical displacement. The left side of the domain is limited by a symmetry condition, while the right side is constrained by a rolling constraint. The entire domain is subjected to gravitational acceleration.

2.2. Simulation implementation

The tunnel excavation model and the simulation of this process were carried out in the Comsol Multiphysics application. Initially, it was established that the analyzed model is of the 2D type, and its stationary analysis (Stationary) will be performed through Structural Mechanics → Solid Mechanics (solid).

2.2.1. Building the model geometry

We used the Rectangle primitive from the Geometry menu, with the numerical values from Figure 6, which refer to the width, height, and the position of the bottom-left corner of the rectangle. By executing the Build Selected command, the first part of the geometry was drawn.

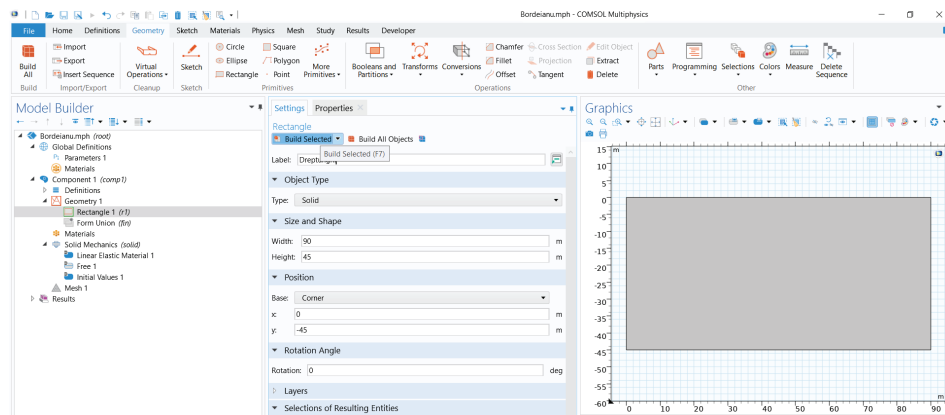


Fig. 6. Drawing the rock mass

Also from the Geometry menu, but using the Circle primitive this time, a semicircle was drawn according to the values in Figure 7, which corresponds to the part on the right side of the tunnel's symmetry axis.

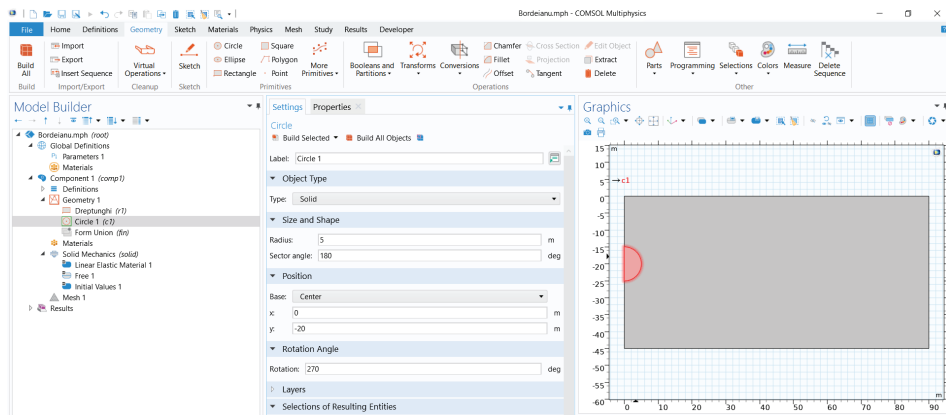


Fig. 7. Drawing the right half of the tunnel's symmetry axis

The geometry construction of the model is considered completed after activating Build Selected button in the Form Union.

2.2.2. Setting the options for solid mechanics

Since the Poisson's ratio is close to 0,5 a mixed formulation will be used for the material's linear elastic properties. To do this, in Component 1 (comp1) → Solid Mechanics (solid) select Linear Elastic Material 1. Then, for the corresponding list under Use mixed formulation choose Pressure formulation.

2.2.3. Setting the symmetry

In the Physics window for Boundaries select the Symmetry option. This defines the axis of symmetry as shown in Figure 8.

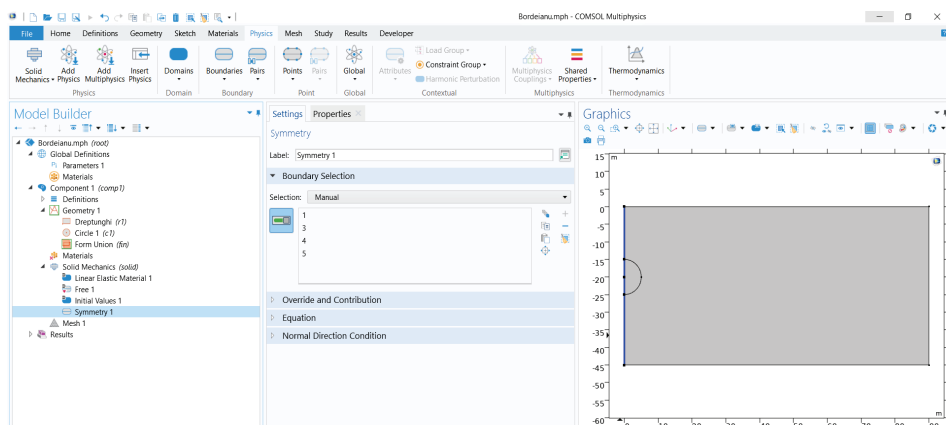


Fig. 8. Setting the axis of symmetry

2.2.4. Setting the constraints

In the Physics window for Boundaries, the Fixed Constraint option was selected first to establish the fixed elements of the model (Figure 9), and the Roller option was selected to define the parts of the model with a rolling constraints (Figure 10). For the Free option was chosen (Figure 11). For the Free option was chosen (Figure 11).

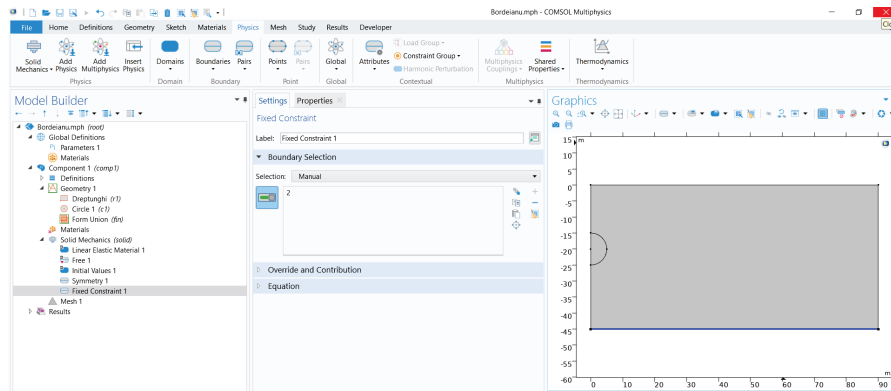


Fig. 9. Setting the fixed constraints

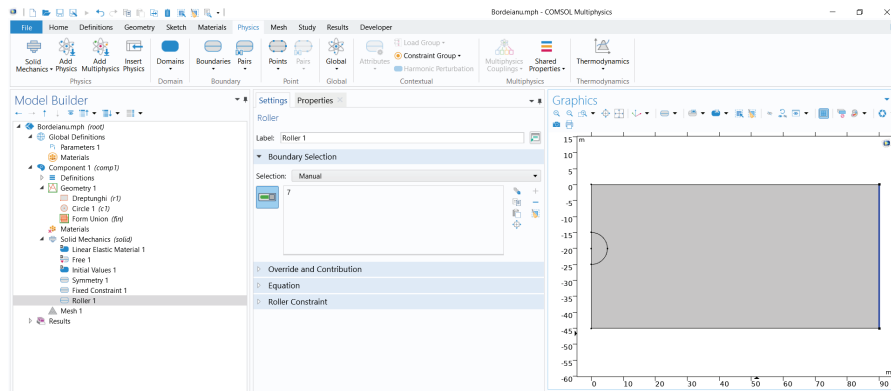


Fig. 10. Setting the rolling constraint

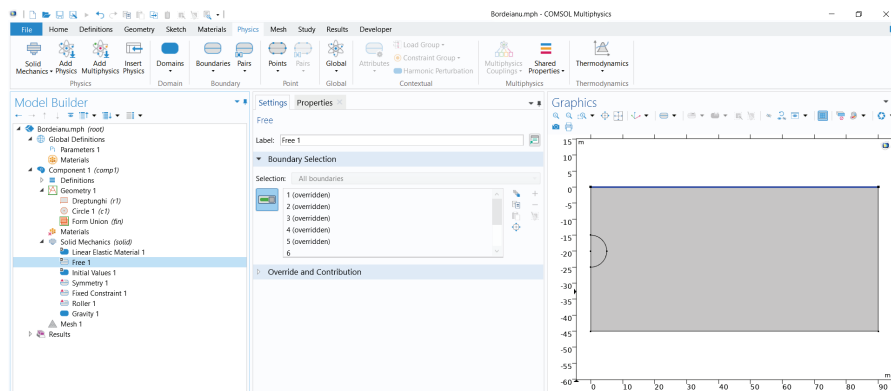


Fig. 11. Setting the free parts of the model

In the Physics window, for the Domain option, Gravity is selected.

2.2.5. Setting the soil plasticity

In the Physics window, under the Attributes option, Soil Plasticity is selected. For the corresponding Soil Plasticity settings, the option Match to Mohr-Coulomb criterion is activated. Additionally, in the Physics window and under the Attributes option, Initial Stress and Strain is selected. In the setting window for Initial Stress and Strain the expressions S_0 for the stress and strain are entered in the corresponding matrix in Figure 12.

Initial Stress and Strain		
Initial stress:		
S_0	<code>withsol('sol1', solid.sx)</code> <code>withsol('sol1', solid.sxy)</code> <code>withsol('sol1', solid.sxz)</code>	<code>withsol('sol1', solid.sxy)</code> <code>withsol('sol1', solid.sy)</code> <code>withsol('sol1', solid.syz)</code>
		<code>withsol('sol1', solid.sxz)</code> <code>withsol('sol1', solid.syz)</code> <code>withsol('sol1', solid.sz)</code>
		N/m ²
Initial strain:		
ϵ_0	0 0 0	0 0 0
		1

Fig. 12. Setting the expression for stress and relative deformation

Next, an Activation node will be added to the material's elastic properties in order to model the removal of the soil. To do this, in the Physics window under the Attributes option, Activation is selected. In the Activation properties window, only the part of the domain that will remain after excavation is selected. In the Activation field, the Scale factor value $1 \cdot 10^{-9}$ is entered.

2.2.6. Soil material properties

In Component 1 (comp1), the Blank Material option is selected under Materials. For the Contents section option, the values corresponding to Figure 13 are entered.

Material Contents					
Property	Variable	Value	Unit	Property group	
<input checked="" type="checkbox"/> Young's modulus	E	12[MPa]	Pa	Young's modulus and Poisson's ratio	
<input checked="" type="checkbox"/> Poisson's ratio	nu	0.495	1	Young's modulus and Poisson's ratio	
<input checked="" type="checkbox"/> Density	rho	2000	kg/m ³	Basic	
<input checked="" type="checkbox"/> Cohesion	cohesion	130[kPa]	Pa	Mohr-Coulomb	
<input checked="" type="checkbox"/> Angle of internal friction	internalphi	30[deg]	rad	Mohr-Coulomb	

Fig. 13. Material properties

2.2.7. Finite element mesh

In the Mesh bar, the Free Triangular option is selected. The finite element size will be of the Finer type. For Free Triangular 1, Distribution is selected. Here, the limits 8 and 9, which represent the boundary between the remaining massif and the excavated area, are added. For these, the value 12 is set in Number of elements. The resulting finite element mesh is shown in Figure 14.

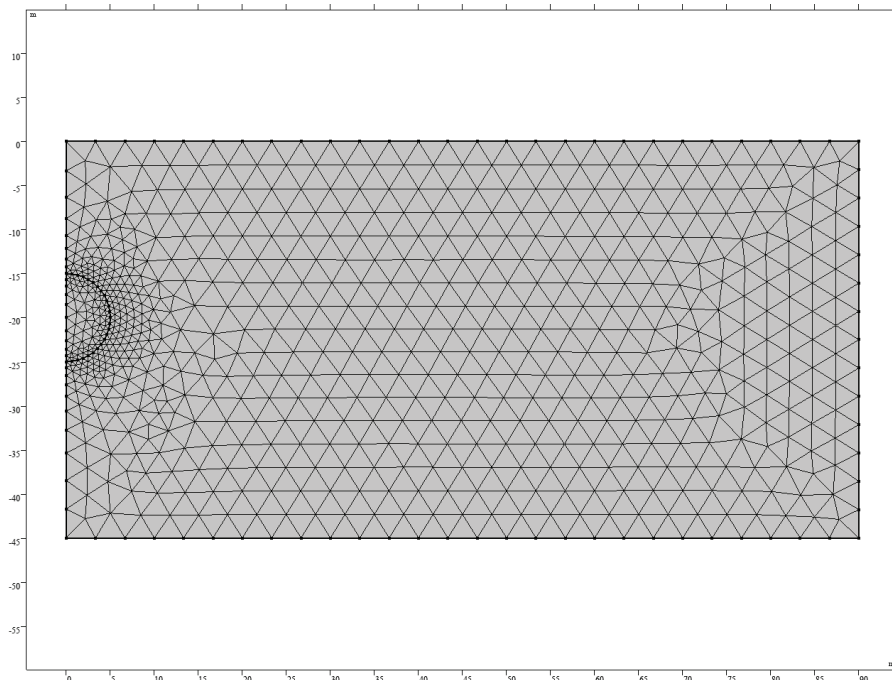


Fig. 14. Finite element mesh

3. RESULTS

3.1. Results before excavation

First, the results related to the in situ stress caused by the action of gravitational acceleration are presented. Thus, in Figures 15, 16, and 17, the loading per unit volume, deformation, and stress before excavation are shown. The results obtained are due to the action of gravity, and the maximum values are in accordance with the geomechanical characteristics, and the material properties of the model being simulated.

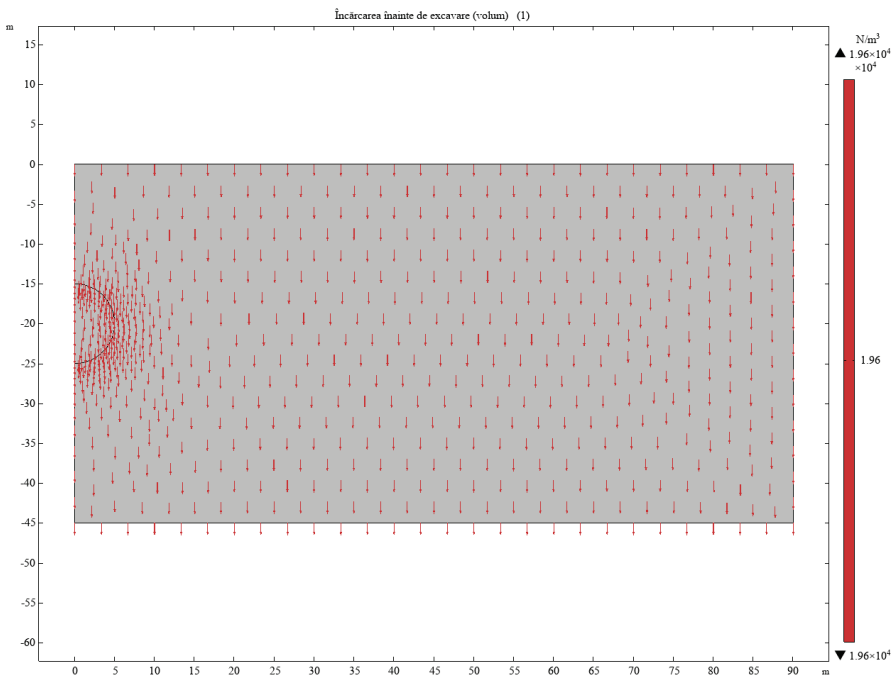


Fig. 15. Volumetric loading of the massif before excavation

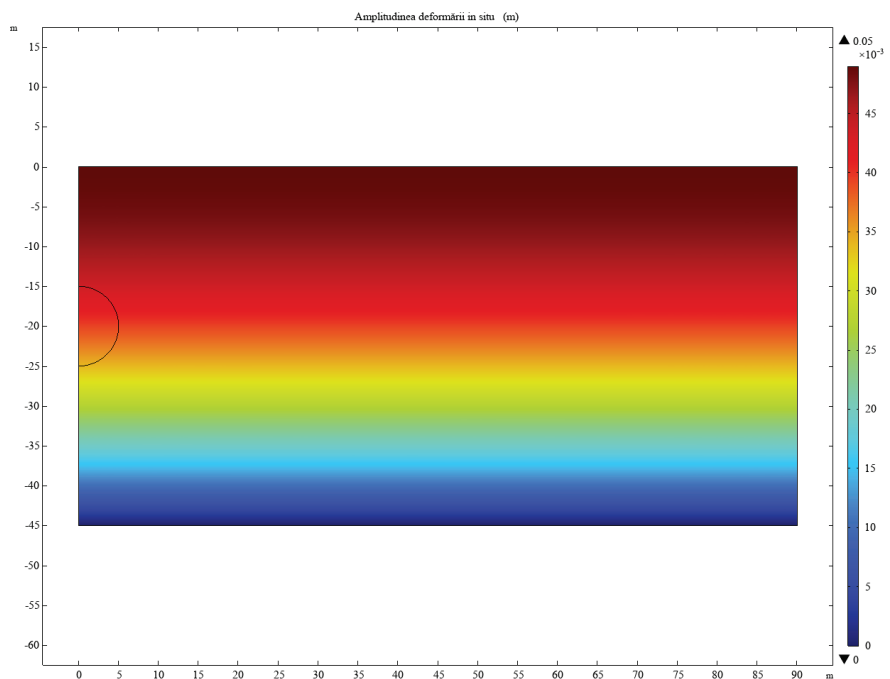


Fig. 16. In situ deformation of the model subjected to simulation

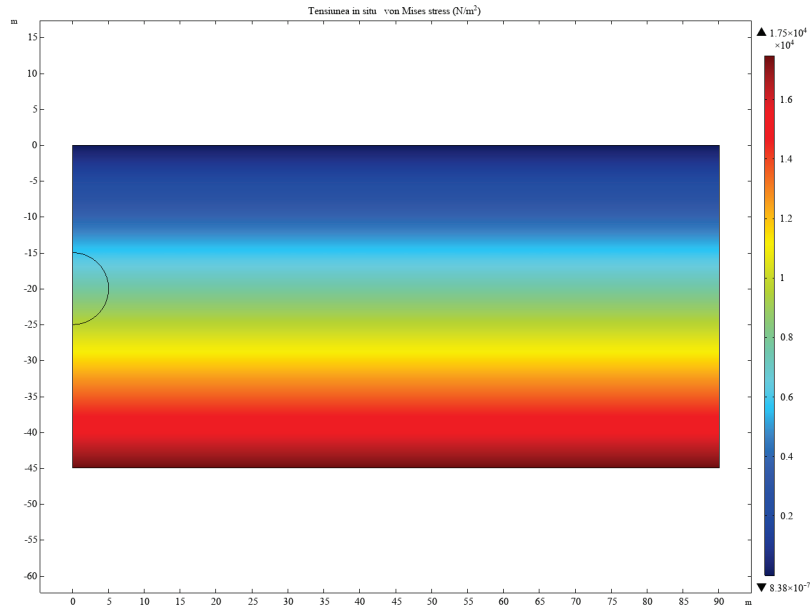


Fig. 17. In situ stress in the model subjected to simulation

3.2. Results after excavation

Figure 18 shows the volumetric loading of the massif after excavation.

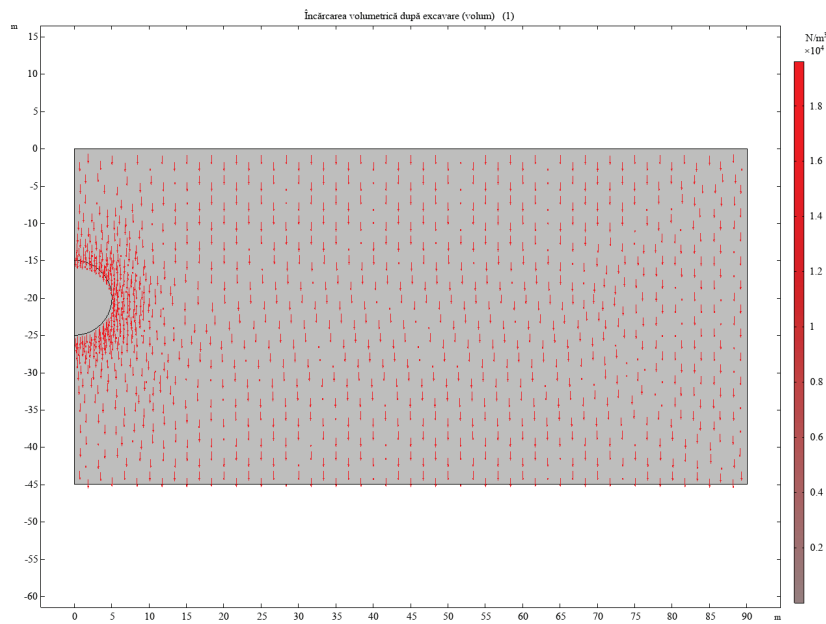


Fig. 18. Volumetric loading of the massif after excavation

Figure 19 highlights the magnitude of the deformation, while Figures 20 and 21 show the displacement along the X and Y directions, respectively, following the tunnel excavation.

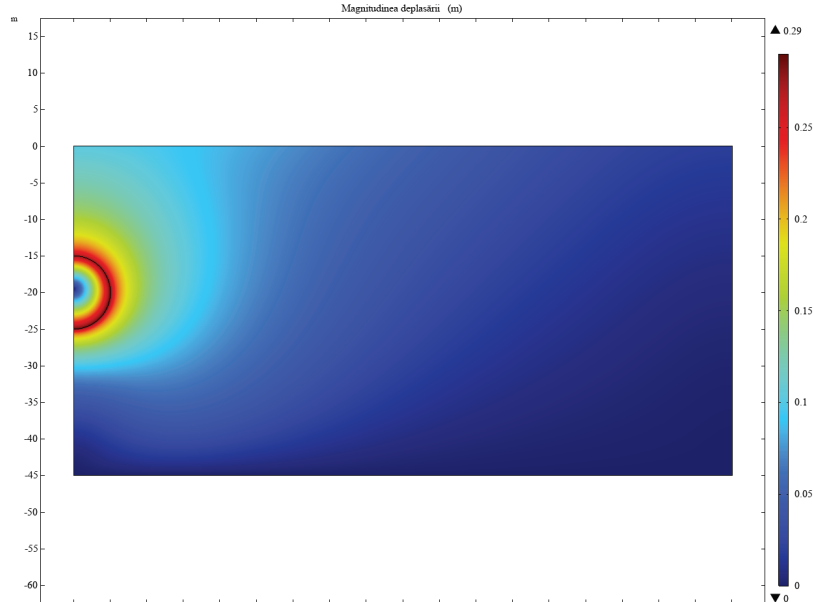


Fig. 19. Magnitude of displacement after excavation

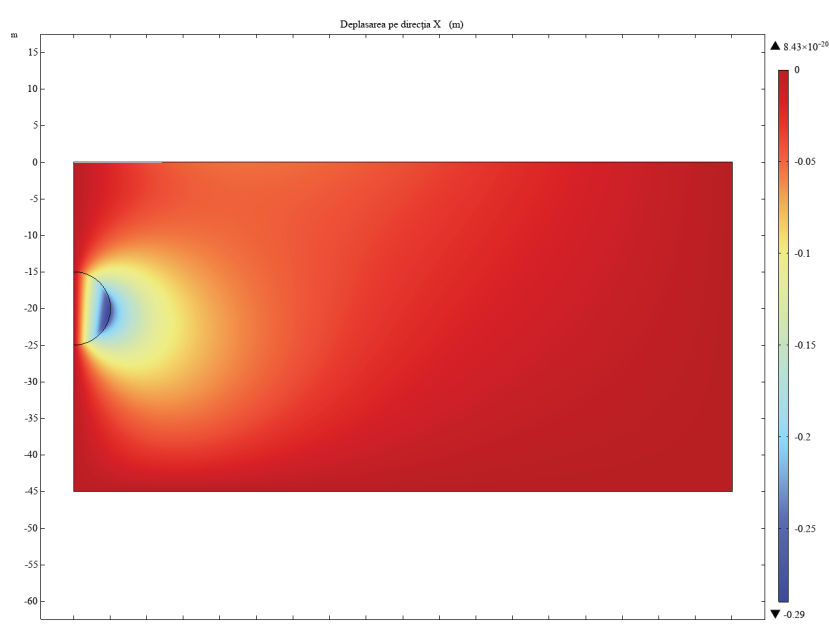


Fig. 20. Displacement along the X direction after excavation

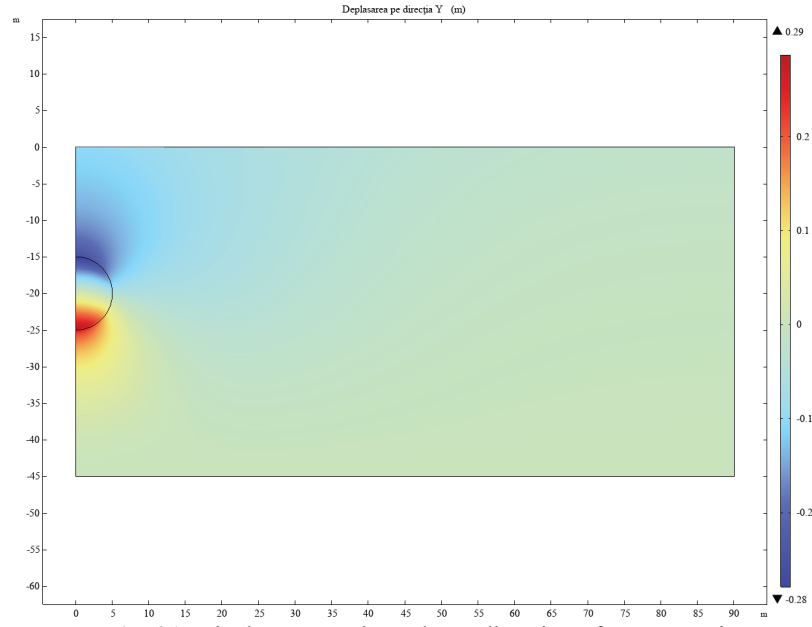


Fig. 21. Displacement along the Y direction after excavation

The stress established in the massif after the tunnel excavation is shown in Figure 22. Figure 23 highlights the plastic behavior at two levels due to the excavation.

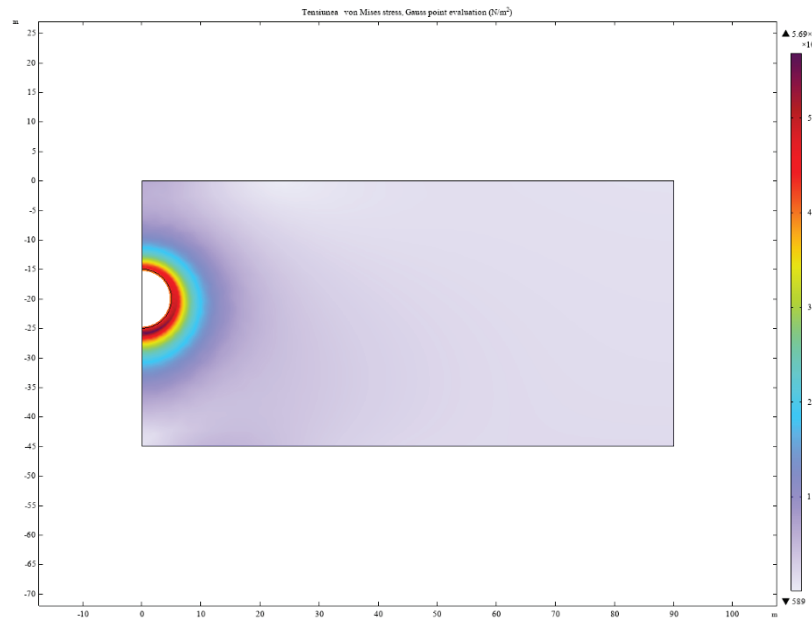


Fig. 22. The stress after the tunnel excavation

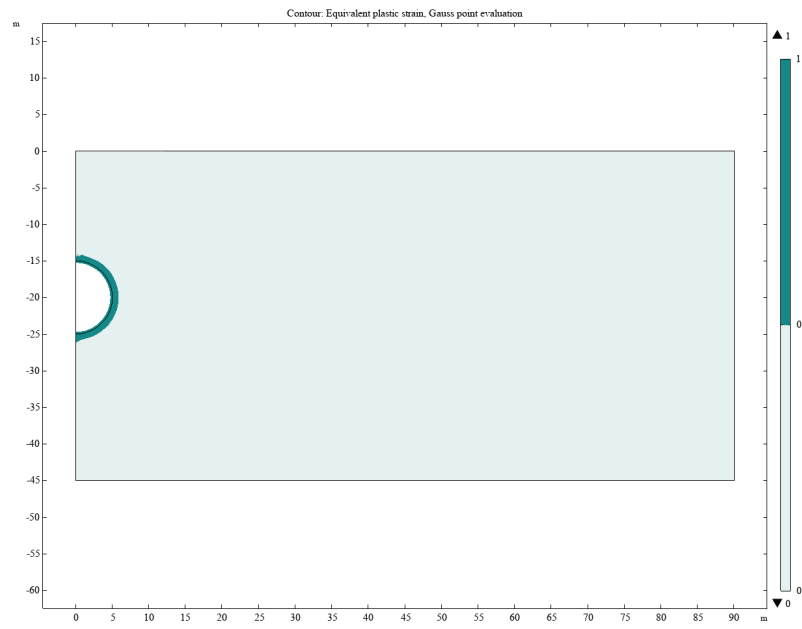


Fig. 23. The plastic behavior at two levels of the massif

Figures 24 and 25 show the displacement in the X and Y directions of the three part of the model subjected on the simulation.

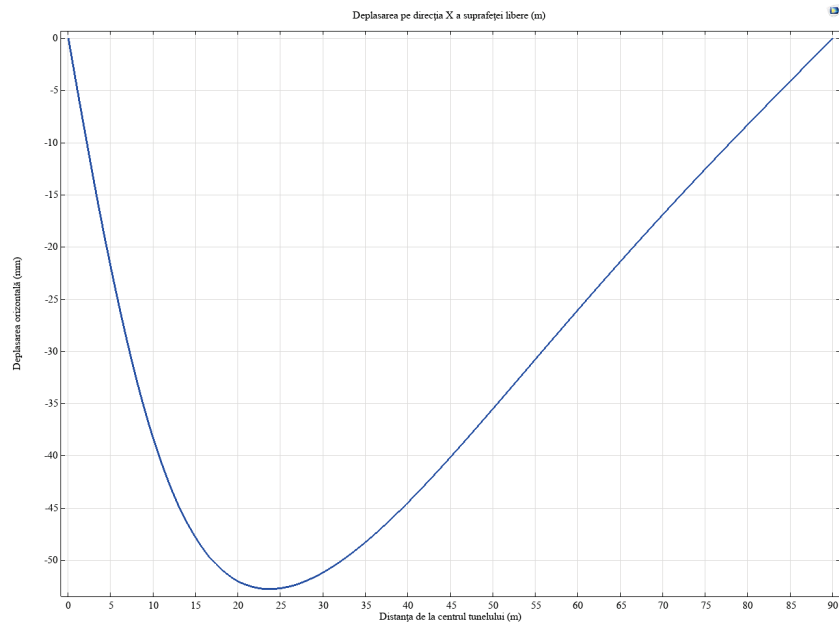


Fig. 24. Displacement in the X direction of the free components of the model

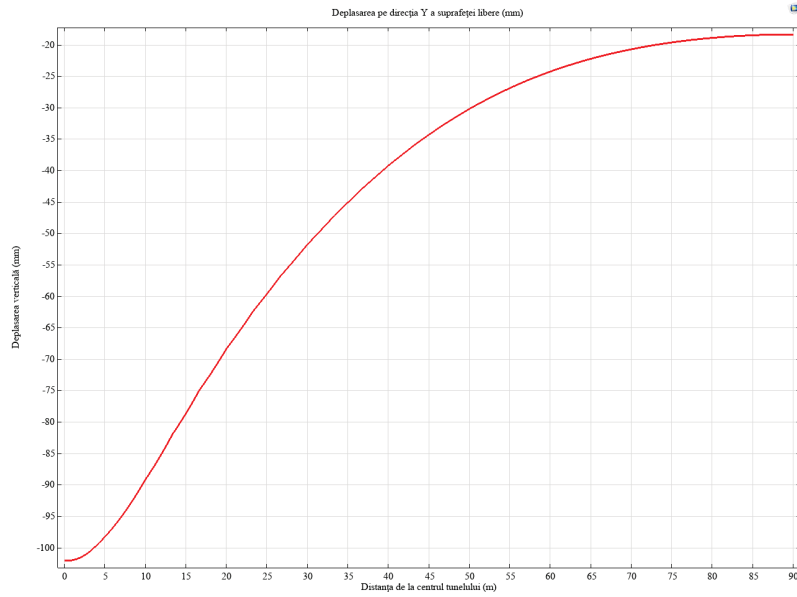


Fig. 25. Displacement in the Y direction of the free components of the model

To provide a more suggestive view of the results obtained after excavation, we used the extrusion feature offered by the Comsol application to create a 2D image of the simulation results. Figures 26 and 27 show the extruded image of the deformation and the von Mises in the model subjected to the simulation.

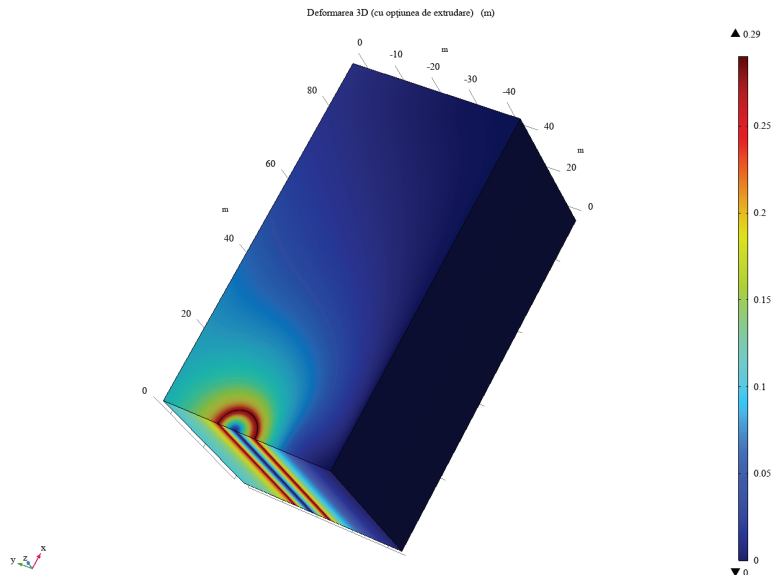


Fig. 26. Deformation of the model subjected to the simulation (extruded image)

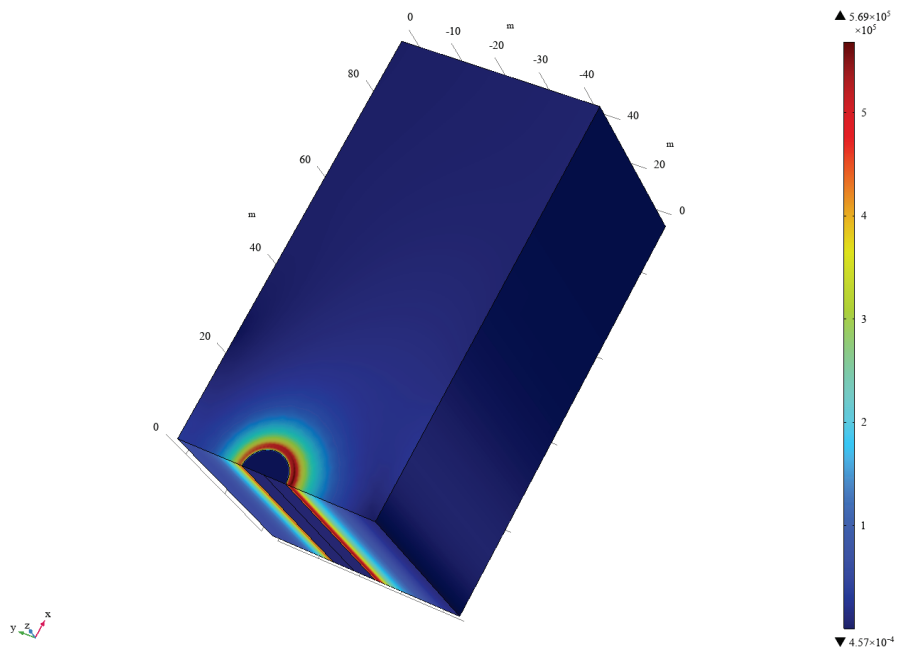


Fig. 27. Von Mises stress in the model subjected to the simulation (extruded image)

CONCLUSIONS AND DISCUSSIONS ON THE RESULTS OBTAINED

It can be observed that the boundaries of the model domain subjected to simulation, the roller surfaces, and the symmetry determined by the axis of symmetry induce a linear variation in the vertical direction of the von Mises stress.

In the second part of the simulation, besides tunnel excavation, a soil plasticity feature was introduced. This presents, at two levels, the region that undergoes plastic deformation.

It can be observed that tunnel excavation leads to a modification of the stress and deformation equilibrium in the excavated massif, causing the accumulation of stresses and the increase of deformations at the tunnel wall boundary.

The horizontal axis of symmetry of the tunnel shows deformations both in the X direction and in the Y direction. It is noted that the deformation along the horizontal axis increases up to the tunnel wall boundary, which is located 5 meters from the vertical axis. At the extreme right boundary of the model, the deformation reaches a value of 0, as it is not affected by the tunnel excavation.

The use of the Comsol 3D extrusion feature for 2D results provides a much better perception of the geomechanical phenomena that occur following tunnel excavation.

REFERENCES

- [1]. COMSOL Multiphysics 6.0, Tunnel Excavation
- [2]. **Popescu, F. D., Radu, S. M., Kotwica, K., Andraş, A., Kertesz, I.** *Simulation of the time response of the ERc 1400-30/7 bucket wheel excavator's boom during the excavation process.* Sustainability, 11(16), 4357, 2019.
- [3]. **Sapigni, M., Berti, M., Bethaz, E., Busillo, A., Cardone, G.** *TBM performance estimation using rock mass classifications.* International Journal of Rock Mechanics and Mining Sciences 39, no. 6 (2002): 771-788.
- [4]. **Popescu, F.D., Radu, S.M., Andras, A., Brinas, I.K.** *A grafo-numeric method of determination of the operation power of the rotor of EsRc-1400 bucket wheel excavator using computer simulation in SolidWorks.* MATEC Web Conf. 290, 04007, 2019.
- [5]. **Tomus, O.B., Andraş, A., Andraş, I.** *Study of the dependence between the cutting direction relative to stratification and the digging characteristics of lignite in oltenia coal basin (Romania),* 17th International Multidisciplinary Scientific GeoConference ISBN 978-619-7105-00-1 / ISSN 1314-2704, vol. 17, Issue 13, 825-830, 2017. DOI: 10.5593/sgem2017/13/S03.104.
- [6]. **Popescu, F.D.** *Instalații de Transport pe Vertical;* Editura Focus: Petroșani, Romania, 2010.
- [7]. **Radu, S.M., Popescu, F.D., Andras, A., Kertesz, I.** *Transport si instalații miniere,* Editura Universitas, Petroșani, 2018, ISBN 978-973-741-587-5
- [8]. **Popescu, F.D., Aplicații industriale ale tehnicii de calcul,** Editura AGIR, București, 2009.
- [9]. **Kovacs., I.; Andras, I.; Nan, M.S.; Popescu, F.D.** *Theoretical and experimental research regarding the determination of non-homogenous materials mechanical cutting characteristics.* In Proceedings of the 8th Conference on Simulation, Modelling and Optimization (SMO), Santander, Cantabria, Spain, 23–25 September 2008; pp. 232–235.
- [10]. **Popescu, F.D., Radu, S.M.** *Vertical Hoist Systems: New Trends Optimizations.* LAP Lambert Academic Publishing, 2013.
- [11]. **Andraş, A., Brînaş, I., Radu, S.M., Popescu, F.D., Popescu, V., Budilică, D.I.** *Investigation of the Thermal Behaviour for the Disc-Pad Assembly of a Mine Hoist Brake Using COMSOL Multiphysics.* Acta Tech. Napoc.-Ser. Appl. Math. Mech. Eng. 64, 227–234, 2021.
- [12]. **Nan MS, Kovacs J., Popescu FD.** *Balance control by weighing and tensiometric measurements of bucket wheel excavators,* “WSEAS Transactions On Systems And Control” 2008, 11, 3: 927–936.
- [13]. **Andras, I., Radu, S. M., Andras, A.** *Study Regarding the Bucket-Wheel Excavators Used in Hard Rock Excavations,* Annals of the University of Petroșani, Mechanical Engineering, Vol. 18, pp. 11-22, 2016.
- [14]. **Radu, S. M., Popescu, F. D., Andras, A., Kertesz (Brînaş), I., Tomus, O. B.** *Simulation and modelling of the forces acting on the rotor shaft of BWES, in order to improve the quality of the cutting process.* Annals of the University of Petroșani, Mechanical Engineering, Vol. 20, pp. 63-72, (2018).
- [15]. **Popescu, F.D.** *Calculatorul numeric în industria extractivă,* Editura Universitas, Petroșani, 2004.
- [16]. **Yin, L. J., Gong, Q. M., Zhao, J.** *Study on rock mass boreability by TBM penetration test under different in situ stress conditions.* Tunnelling and Underground Space Technology, 43, 413-425, 2014.

-
- [17].**Popescu, F. D., Radu, S.M., Andras, A., Kertesz, I.**, *Infografică, modelare și simulare asistată de calculator*, Editura Universitas, Petroșani, 2020, ISBN:978-973-741-714-5.
 - [18].**Popescu, F. D., Radu, S.M., Andras, A., Kertesz, I.**, *Infografică, modelare și simulare asistată de calculator –format electronic*, Editura Universitas, Petroșani, 2020, ISBN 978-973-741-715-2.
 - [19].**Fang, X., Yang, J., Zhang, X., Zhang, C., Wang, S., Xie, Y.** *Numerical modeling of open TBM tunneling in stratified rock masses using a coupled FDM-DEM method*. Computers and Geotechnics, 156, p.105251, 2023.
 - [20].**Sakcali, A., & Yavuz, H.** *Prediction of the longitudinal ground pressure-acting roof of the shield during single-shield TBM excavation in weak rock masses*. Bulletin of Engineering Geology and the Environment, 81(11), 477, 2022.
 - [21].**Lisjak, A., Mahabadi, O. K., Kaifosh, P., Vietor, T., Grasselli, G.** *A preliminary evaluation of an enhanced FDEM code as a tool to simulate hydraulic fracturing in jointed rock masses*. In ISRM EUROCK (pp. ISRM-EUROCK). ISRM, May 2014.
 - [22].**Doroodian, B., Ahangari, K., Noorzad, A.** *Damage caused by mechanized tunnel boring in high-stress hard rock*. Transportation Geotechnics, 34, 100741, 2022.